Tectonophysics 799 (2021) 228690

Contents lists available at ScienceDirect

Tectonophysics

journal homepage: www.elsevier.com/locate/tecto

Co-seismic beachrock deformation of 8th century AD Earthquake in Middle Strand of North Anatolian Fault, Lake Iznik, NW Turkey

Ahmet Evren Erginal [a,*], Ramazan Cüneyt Erenoğlu [b], Cengiz Yıldırım [c], H. Haluk Selim [d], Nafiye Güneç Kıyak [e], Oya Erenoğlu [a], Emin Ulugergerli [f], Mustafa Karabıyıkoğlu [g]

[a] Çanakkale Onsekiz Mart University, Faculty of Education, Department of Geography Education, Çanakkale 17100, Turkey
[b] Çanakkale Onsekiz Mart University, Faculty of Engineering, Department of Geomatics Engineering, Çanakkale 17100, Turkey
[c] Istanbul Technical University, Eurasia Institute of Earth Sciences, Istanbul 34469, Turkey
[d] Istanbul Gelişim University, Department of Civil Engineering, Istanbul 34310, Turkey
[e] Istanbul OSLAB- Research & Archeometry Group, Istanbul, Turkey
[f] Çanakkale Onsekiz Mart University, Faculty of Engineering, Department of Geophysical Engineering, Çanakkale 17100, Turkey
[g] Ardahan University, Faculty of Humanities and Letters, Department of Geography, Ardahan 75000, Turkey

ARTICLE INFO

Keywords:
North Anatolian Fault
Middle Strand
Lake Iznik
Paleoseismology
AD 715
Beachrock

ABSTRACT

A historical earthquake-related co-seismic deformation observed on beachrock beds along the southern shoreline of Lake Iznik is discussed as a new paleoseismic record for an 8th century AD earthquake in the Middle Strand of the North Anatolian Fault, NW Turkey. Electrical Resistivity Tomography (ERT) images beneath the beachrock surface allowed monitoring of the subsurface trace of a normal fault dipping north along a 100 m surface rupture. No strike-slip deformation exists along the rupture, suggesting that the deformation in the beachrock is connected with a secondary structure, and that the main surface rupture was under the lake waters. The deformed beds of the beachrock, dated using Optically Stimulated Luminescence (OSL) to 1.3 ± 0.15 ka, are overlain by an undeformed secondary deposition of beds dated to 1.2 ± 0.09 ka. This allows us to narrow down the time of the faulting and implying that it was most likely a result of the AD 715 earthquake.

1. Introduction

Understanding the earthquake history of bifurcated major fault zones such as the North Anatolian Fault Zone (NAFZ) in the Eastern Marmara Region is one of the major challenges in paleoseismology because of the complex nature of slip-partitioning among the closely-spaced fault strands. In this tectonic setting, the presence of evident slip rate differences (Reilinger et al., 2006) between the northern strand (24 ± 0.1 mm/yr) and the middle strand (0.8 ± 0.1 mm/yr) gives rise to differences in seismic cycles. The northern strand generates earthquakes with shorter recurrence intervals (250–300 yr) in proportion to the middle strand (Şengör et al., 2005; Kozacı et al., 2011). The spatial proximity of these strands has caused the destruction of settlements along both strands, making it complicated to assess historical records in terms of identifying the source fault. Most of the paleoearthquakes were assigned to the northern strand because of its higher slip-rate, but the destruction of Iznik (Nicea), one of the largest ancient cities in the region, indicates the occurrence of large earthquakes along the middle strand as well.

Historical records reveal that in AD 29, 33, 69, 120, 368, 378, 715 and 740, earthquakes damaged the city of Iznik (Pınar Erdem and Lahn, 2001; Ergin et al., 1967; Soysal et al., 1981; Ambraseys, 2002; Ambraseys and Finkel, 1991; Ambraseys and Jackson, 1998; Guidoboni et al., 1994; Adatepe and Erel, 2006; Fraser et al., 2010; Özalp et al., 2013). Recently discovered sunken church walls under the lake surface have been linked to the AD 740 earthquake by underwater archaeological data (Şahin et al., 2014a, 2014b). On the other hand, geological evidence of these earthquakes still lacks current field data. Paleoseismological data from the town of Gemlik (15 km west of Lake Iznik shoreline (Fig. 1) reveal traces of the AD 1857 and 1419 earthquakes (Özalp et al., 2013; Ikeda et al., 1991). Geological evidence of an earlier earthquake that occurred in AD 1296 was found (Soysal et al., 1981; Ambraseys, 2002) in the eastern part of the middle strand around the town of Geyve (approx. 50 km east of Lake Iznik shoreline).

The only persuasive paleoseismic evidence for the AD 740 earthquake comes from the Kaynarca site located 10 km east of Lake Iznik. A

* Corresponding author.
E-mail address: aerginal@comu.edu.tr (A.E. Erginal).

https://doi.org/10.1016/j.tecto.2020.228690
Received 23 May 2020; Received in revised form 28 October 2020; Accepted 19 November 2020
Available online 23 November 2020
0040-1951/© 2020 Elsevier B.V. All rights reserved.

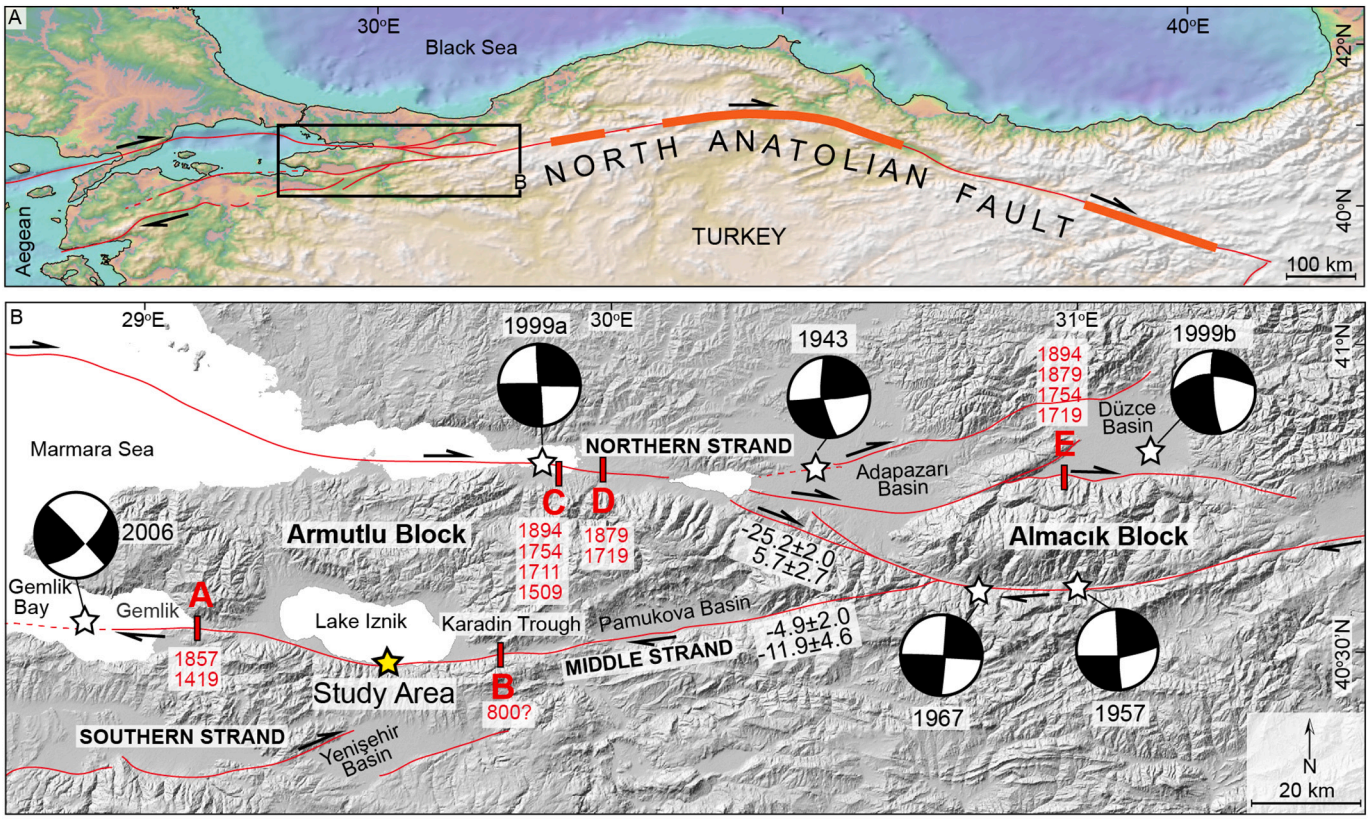

Fig. 1. (a) Location map of study area, and (b) threads from north to south in North Anatolian Fault Zone.

minimum paleomagnetic age of 1200 years, based on the analysis of pipe fragments embedded within a clayey unit, suggested that the AD 740 event was the only earthquake in the last 4130 ± 500 years (Barka, 1993). Since the temporal resolution of this dating is not very high, it might be that another earthquake occurred in the 8th century AD. The slower slip rate of the middle strand makes it difficult to preserve surface ruptures and is also an impediment to extracting information from conventional paleoseismic trenching in the middle strand (Barka, 1993; Özalp et al., 2013). This fuzzy situation increases the significance of our contribution, where we provide geological and geomorphological evidence of a co-seismic surface deformation associated with an earthquake. This is the first onshore surface rupture report associated with the middle strand of the NAF.

In this study, we focused on the beachrocks of Lake Iznik, which are sensitive geomorphic markers of Holocene lake level changes as well as co-seismic deformation. The southern shore of the lake is unique in terms of the wide distribution of well-developed beachrock formations along the shoreline (Kayan, 1996; Erginal et al., 2012a, 2012b; Öztürk et al., 2016). Beachrocks are loose beach materials of different sizes cemented in the intertidal zone to form beds dipping toward the sea or

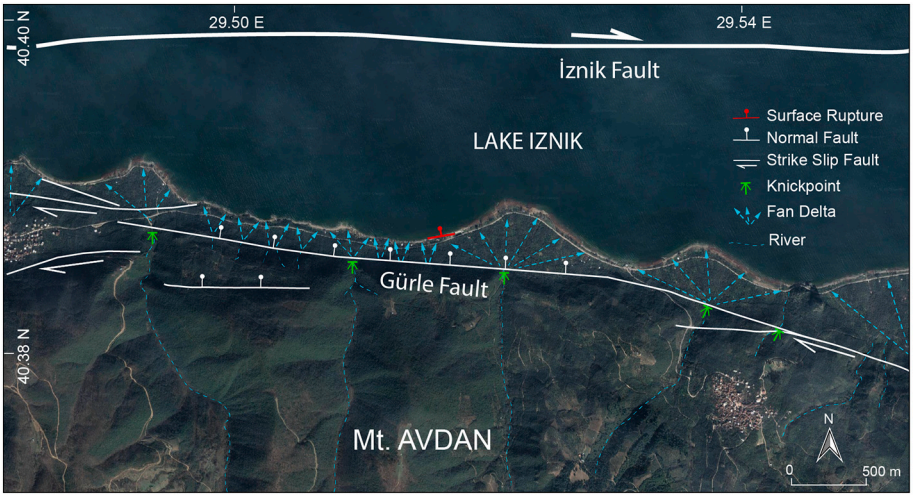

Fig. 2. Gürle Fault and alluvial fan deltas on southern shores of Lake Iznik (Fig. 2). Lower image taken from Google Earth. The active subaquatic fault after Gastineau et al. (2020).

lake at angles varying between 5° and 10° and with ages varying between 1 and 5 ka (Vousdoukas et al., 2007 and references therein). These properties of beachrock provide key references for us to quantify Holocene sea/lake level changes and also active coastal tectonics (Bezerra et al., 1998; Kelletat, 2006). In this paper, the differences in dips between the deformed and undeformed beach layers were considered to quantify co-seismic displacement. Optically Stimulated Luminescence (OSL) was used to constrain the timing of the earthquake and Electrical Resistivity Tomography (ERT) imaging was applied to understand the subsurface geometry and kinematics of the surface rupture. We also wish to make a contribution to discussion on the submergence of the so-called St. Neophytos basilica on the eastern shore of the lake, which has previously been assigned to the destructive AD 740 earthquake.

2. Regional setting

The freshwater Lake Iznik is located between latitudes 40°30′–40°22′ N and longitudes 29°20′–29°42′ E in the southeast of the Marmara region of Turkey (Fig. 1). It is the fifth largest lake in Turkey with a maximum length of 32 km and width of 12 km in *E*-W and N-S directions, respectively, and has a surface area of 302.2 km^2. It occupies part of the fault-bounded Iznik depression covering an area of 1426.2 km^2 (Akbulak, 2006), with a drainage network of 1246 km^2 and a water depth of maximum 80 m (Öztürk et al., 2009).

The middle strand delimits the southern margin of the Lake Iznik Basin and is characterized by north-dipping en-echelon transtensional segments within a releasing stepover (Fig. 1b; Öztürk et al., 2009; Emre et al., 2013; Doğan et al., 2015; Gastineau et al., 2020). The deepest part (75 m) of the lake displays an elongated basin geometry close to the southern shore within this releasing stepover. Offshore seismic reflection and multi-beam bathymetry data reveal that a 1 m high south-facing linear fault scarp deforms the lake bottom and stretches parallel to the southern shoreline (Gastineau et al., 2020). The Gürle Fault is one of the major segments of the middle strand (Doğan et al., 2015), delimiting the mountain front of the southern shores (Fig. 2). This part of the shore is characterized by closely-spaced fan deltas. Strongly-cemented beachrock layers stretch along almost all of the shoreline of the fan deltas.

As is the case with most other beachrock deposits on the shores of Lake Iznik, the depositional environment prior to carbonate cementation can be defined as a point-sourced alluvial fan prograding to the lacustrine basin (Erginal, 2017). As a characteristic indicator of the depositional environment prior to cementation, grain-supported sandy conglomerate and coarse sandstone beds with erosional lower contacts represent shallow-braided stream bars and channel fills, indicating subaerial deposition on an alluvial fan. The wave-rippled, ruptured coarse pebbly sandstones imply deposition on the shallow wave-dominated lake shoreline, the water depth of which lay within the limits of the wave base before it was subjected to faulting.

In this tectonic and geomorphic setting, the space-based geodetic slip rate data (Reilinger et al., 2006) reveal that the middle strand is a low strain area characterized by relatively-low seismicity during the instrumental period. There is no large magnitude earthquake recorded along the middle strand in the instrumental period. The focal mechanism solutions of the moderate to low magnitude earthquakes display normal faulting and strike slip faulting (Öztürk et al., 2009).

3. Methodology

3.1. Sampling and analyses

The dip and strike of beachrock beds were measured along topographical profiles extending parallel to the shoreline. Three OSL samples were taken from 3 different locations of beachrock to determine $CaCO_3$ and the moisture content as well as estimating the environmental dose-rate, which was carried out via inductively-coupled plasma mass spectroscopy (ICP-MS) at the facilities of Bureau Veritas in Canada.

Accelerator Mass Spectrometry (AMS) ^{14}C dating of the two samples taken from the tilted beachrock was carried out at the TÜBİTAK Marmara Research Center (MAM), Turkey. Carbonate-bearing bulk samples were not reworked or affected by diagenetic processes. The collected samples were ultrasonicated to clean them from mud, washed in distilled water and dried (at 40 °C) prior to the analysis. The reservoir effect of the Lake Iznik vicinity is calculated as ~370 yrs. (Ülgen et al., 2012; see table 5.1 in Roeser, 2014). All results were calibrated to calendar ages using Calib v7.0 software with an IntCal13.14C calibration curve and reservoir corrections were applied.

3.2. Direct current resistivity survey

A Direct Current Resistivity (DCR) survey is frequently used for near-surface imaging. Electrical Resistivity Tomography (ERT), in particular, is a widely-used DCR technique performed via multi-electrode systems for obtaining both two- and three-dimensional subsurface images. In this study, a DCR survey using ERT was conducted on the southern shore of Lake Iznik. The ERT profile is at the location of carbonate-cemented hard-bedrock beds with a buried thickness of 1 m.

The ERT measurements were carried out at two sites with a local brand instrument with a manual switch box for the multi-electrode survey, using dipole–dipole electrode configuration (Loke, 2004; Neyamadpour et al., 2010). Data from the voltage drop and injected current, and in turn the apparent resistivity, were acquired using 24 electrodes spaced at 1-m intervals in order to depict the subsurface structure and contact relationship of the beachrocks, and also to detect possible discontinuities such as faults, fractures and shear zones. The raw resistivity data were processed using well-known inversion software, RESIS2D (Loke, 2013), to produce resistivity tomograms. The tomographic inversion algorithm is based on smoothness-constrained least-squares used by a quasi-Newton optimization technique (Loke, 2013). The elevation data of the electrodes were also taken into consideration in the inversion processes. The obtained tomograms are presented in the same color range.

3.3. OSL dating: sample preparation, measurements and equivalent dose estimate

Samples were collected from different parts of the beachrock beds to determine the radioactive content, $CaCO_3$ and moisture content for estimation of the environment's dose-rate. To estimate the cosmic ray contribution to the dose and to measure the sampling depth, the elevation and geographical position of each beachrock sample was recorded. After removing the outer surface, the inner portion was crushed and powdered. All laboratory procedures were performed under red-light conditions. The powdered samples were separated by grain size of 90–180 μm under wet sieving prior to the chemical treatment through quartz extraction. Quartz grains were separated after treatment with HCl, H_2O_2 and HF to remove organic matter, $CaCO_3$ and feldspar, respectively. The treatment with HF also removes the outer shell of the quartz grains as it is affected by alpha radiation. The quartz grains were then washed with distilled water and dried in an oven at 50 °C.

For the OSL measurements, the quartz grains were placed on stainless-steel discs using silicon spray. Then ***infrared*** stimulated luminescence (IRSL) measurements with infrared excitation, were taken from the quartz grains and the absence of feldspar was verified. The OSL measurements were carried out with an automated Risø DA-15 TL-OSL system (equipped with an internal 90Sr—90Y beta source giving a dose rate of 89 mGy/s) in the Luminescence Research and Archeometry Laboratory (OSLAB) in Istanbul, Turkey. The optical stimulation was carried out with blue LEDs (470 nm), delivering 40 mW/cm^2 to the sample and luminescence signals were detected using an EMI 9635QA photomultiplier tube fitted with 7.5 mm-thickness Hoya U-340 filters

Table 1
SAR sequence used for OSL dose estimate.

1. Natural (D_n) and Regenerative doses (D_i)
2. Preheat at 260 °C for 10 s
3. Measurement of OSL at 125 °C for 40 s (R_i)
4. Test dose (T_D)
5. TL measurement to 180 °C
6. Measurement of OSL at 125 °C for 40 s (T_i)

(Bøtter-Jensen, 1997). The dose rate of the environment in which the studied samples were buried was derived from U, Th and K concentrations obtained by Inductively Coupled Plasma-emission spectrometry/mass spectrometry (ICP-ES/ICP-MS) analysis.

The conventional single-aliquot regenerative-dose (SAR) protocol used in this study, proposed by Banerjee et al. (1999) and Murray and Wintle (2000), aims to obtain a laboratory dose, namely, an equivalent dose (D_E), producing a luminescence signal equivalent to the natural luminescence signal that the quartz mineral acquired since its last exposure to light. The SAR protocol typically has 6 cycles, as shown in Table 1. Each sample was divided into a number of subsamples (aliquots). Then, a separate D_E value was calculated for each aliquot using the SAR technique. The arithmetic mean of individual D_E values from each sample was considered as the representative D_E value to be used in age calculation.

3.4. Dose rate and OSL ages

The dose rate includes beta and gamma radiation from radioisotopes of potassium, uranium and thorium within the sample and surrounding it, plus external radiation from incoming cosmic rays. External alpha contribution to the dose rates was not considered due to the etching of quartz grains by HF treatment, as described in the sample preparation. Radioelemental analysis was conducted using ICP-MS. The concentration of the radioactive isotopes of U, Th and 40 K were measured by ICP-ES/ICP-MS. Cosmic contribution to the dose rate was calculated using the sampling depth, elevation and geographical position (Olley et al., 1996; Prescott and Hutton, 1988, 1994). All values obtained are presented in Table 2.

OSL age was based on the equivalent dose D_E estimated using the conventional single-aliquot regenerative-dose procedure proposed by Murray and Wintle (2000) on 90–180 μm quartz sand. Dividing the D_E values (in Gy) obtained from each sample by the dose rate (in Gy/ka) yields the OSL age (in ka) related to the geological time since last exposure of the sample to light. The OSL ages and other parameters regarding age calculations are shown in Table 2, where n indicates the number of aliquots evaluated.

4. Results

4.1. Kinematics of deformation

Our co-seismic slip interpretations rely on the deformed beachrocks along the southern shore of Lake Iznik. The original bedding of beachrocks, without tectonic deformation, usually inclines between 5°–10° toward the lake. In our case, we identified three different dips of bedding along a transect normal to the shoreline. The bedding features are distinctly different in the lower, middle and upper sections of the transect. The lakeward (north) dipping lower beds have low angles around 5° where the visible thickness is not more than 20 cm due to wave action. Nevertheless, in the middle section, the dip and dip-direction of the bedding is totally different from the lower and upper parts of the section. Here, the dip of the bedding is 35° and toward the south instead of north.

Table 2
OSL age, equivalent dose, dose rate and other parameters required for dose rate estimates.

Sample code	OSL age (ka)			Equivalent dose (Gy)			n	Dose rate (ka/Gy)			Cosmic	U (ppm)	Th (ppm)	K (%)	CaCO3 (%)	Water content (sat-%)
IZN1	1.3	±	0.15	1.69	±	0.18	12	1.27	±	0.00	0.30	0.5	1.4	0.1	18.09	8.45
IZN2	1.2	±	0.09	1.54	±	0.12	12	1.30	±	0.04	0.30	0.5	1.2	0.11	12.73	8.72

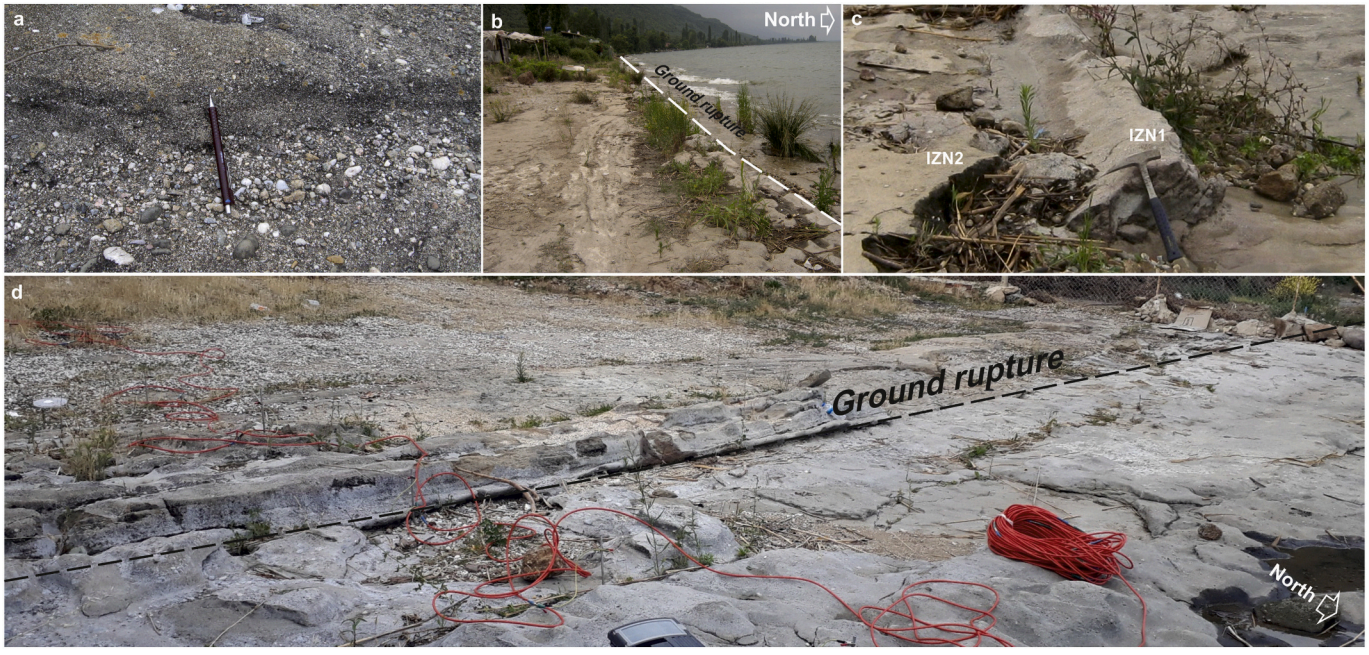

Fig. 3. (a) Close view of beachrock, (b) surface rupture along beachrock zone, (c) back-tilting of beachrock beds, and (d) close view of rupture where ERT measurements were carried out.

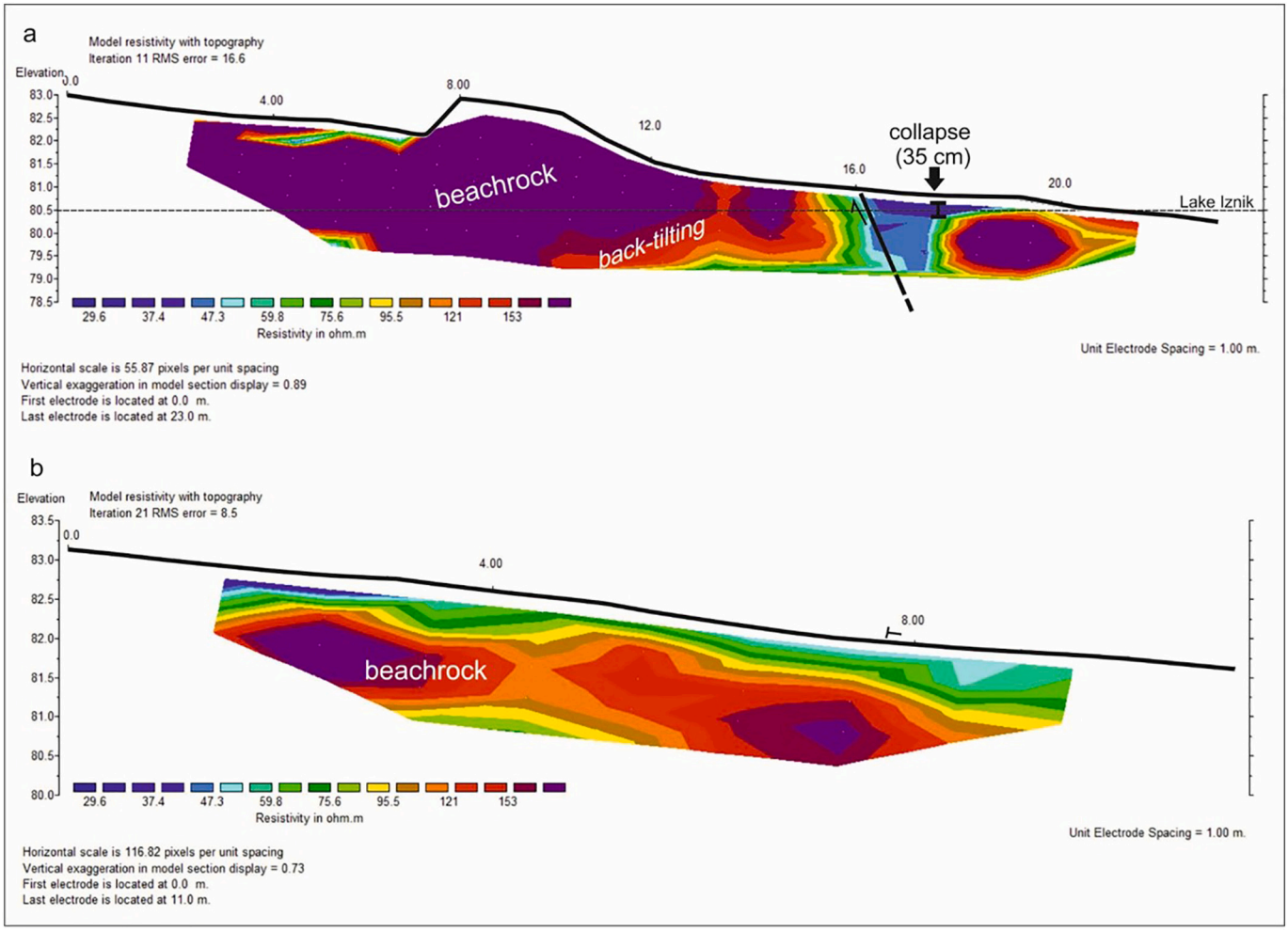

Fig. 4. Two-dimensional ERT images of beachrock beds on (a) southern and (b) eastern shore of Lake Iznik.

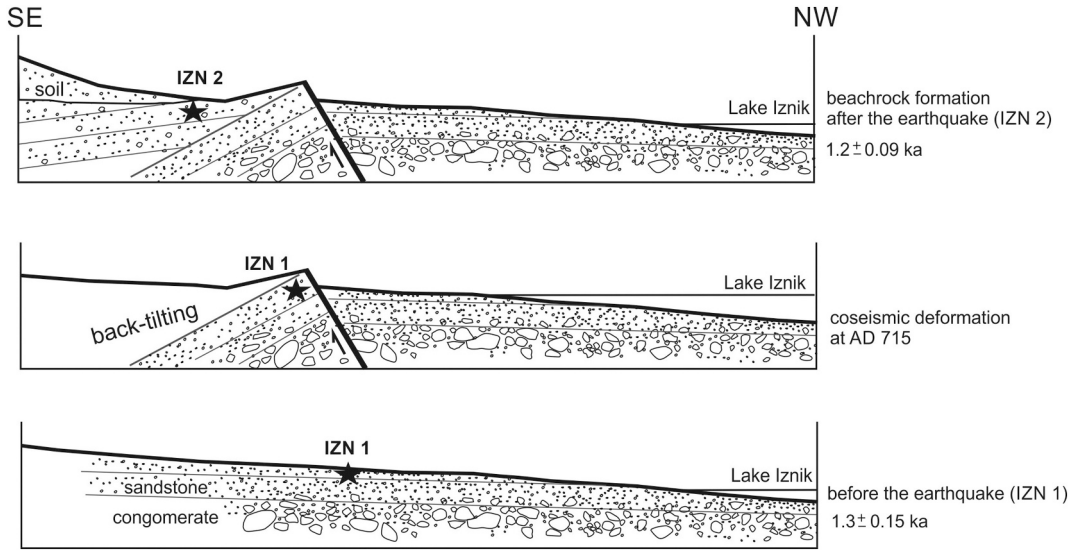

Fig. 5. Conceptual model showing stages of beachrock formation in Lake Iznik.

These back-tilted beachrock beds were overlain by a 20 cm-thick third generation of beachrock with dips of up to 5° toward the south (Fig. 3). The surface expression of this angular unconformity is a subtle scarp that stretches about 100 m parallel to the shoreline.

Our ERT modeling surveys across the deformed beachrock bedding reveal relatively-homogeneous resistivity values ranging from 0 to 160 Ω.m (Fig. 4a). The model also shows a sharp transition of resistivity (60–75 Ω.m) on the surface rupture and reveals sub-surface geometry of

Table 3
Radiocarbon ages obtained from beachrock samples.

Sample code	Uncalibrated age (yrs BP)	Reservoir effect (yrs) (Roeser, 2013)	Calibrated age (cal yrs. BP)
Tübitak-0749 (IZN1)	1734 ± 31	370 ± 100	1299 ± 40
Tübitak-0750 (IZN1)	1512 ± 30	370 ± 100	1034 ± 62

a north-dipping (45°) normal fault plane. This angular unconformity between beachrock beds and the 50 cm-high scarp is the result of a ~50 cm co-seismic dip-slip accommodated by a north-dipping normal fault. In fact, the Gürle Fault that delimits the mountain front also displays characteristics of normal faulting (e.g. triangular facets) in comparison to strike-slip faulting. The absence of strike-slip deformation along the surface rupture indicates that this was a secondary structure away from the main fault or part of a releasing step-over or bend, most probably under the lake, which fits well with recently-published offshore seismic reflection data (Gastineau et al., 2020). Accordingly, our surface rupture may correspond to a fault segment within the negative flower structure suggested by the Gastineau et al. (2020).

4.2. Timing of the deformation

The OSL and AMS ^{14}C dating estimations allow us to constrain a confident timing of the event. The OSL age of the 50 cm-thick deformed (back-tilted) beachrock (Fig. 5) yielded an optical age of 1.3 ± 0.15 ka, which is confirmed by calibrated AMS ^{14}C ages of 1299 ± 40 and 1034 ± 62 years BP (Table 3), considering a reservoir effect of 370 ± 100 (Roeser, 2014). The second generation of beachrock, dated using OSL to 1.2 ± 0.09 ka (IZN 3 in Fig. 5), overlays the deformed bed. These very close ages allow us to bracket the timing of the earthquake to around the 8th century AD. According to historical records, these ages infer that the AD 740 or 715 earthquakes struck Iznik city, as discussed below.

5. Discussion

5.1. AD 740 or AD 715?

The earthquake of 26 October 740 was felt in the whole Marmara and Thrace region, compared to previous earthquakes. It was a significant event also for the Orthodox Church, for every year thereafter they commemorated this earthquake as it was believed to be God's punishment of the iconoclast emperor Leo III the Isaurian (https://www.oca.org/saints/lives/2016/10/26/103060-commemoration-of-the-great-earthquake-at-constantinople). The city walls of Istanbul together with many buildings were damaged and/or collapsed during this earthquake. Historians such as Theophanes the Confessor (circa 752–818) and George Cedrinos (11/12th century) reported that many towns were flooded by tsunami waves (Antonopoulos, 1980).

These historical data invoke the necessity of it being an offshore earthquake. Strike slip faults can only generate a tsunami if they have an evident dip-slip component sufficient to move the water column above; or else they trigger a large landslide which causes a tsunami. It is very difficult for such a large tsunami to be generated by an earthquake occurring along the onshore part of the middle strand. Therefore, we believe that the AD 740 earthquake occurred on the northern strand, most probably in the Marmara Sea, instead of the middle strand. Nevertheless, the foremost earthquake causing great damage to Iznik and several cities around Iznik was the AD 715 event, with a severity of IX (Ergin et al., 1967; Soysal et al., 1981; Guidoboni et al., 1994; Pınar Erdem and Lahn, 2001). We believe that the age of the co-seismic beachrock deformation we found provides geological evidence of the AD 715 earthquake occurring on the middle strand of the North Anatolian Fault instead of AD 740, as previously proposed by Barka (1993) and Şahin et al. (2014a, 2014b).

Fig. 6. Aerial photograph of St. Neophytos Basilica (after Şahin et al., 2014b), displaying the city of Iznik in part and the submerged basilica in the foreground.

5.2. Archeo-seismological implications – submergence of the Byzantine basilica

One of the important archaeological discoveries of the last decade in this region was a submerged basilica close to the east side of Lake Iznik. During a 2014 aerial photo survey, the St. Neophytos basilica, an early Christian structure, was coincidentally discovered under water in Lake Iznik 20 m from the shore at an average depth of 2 m. Based on evidence gathered from underwater archaeological research, the construction of this building, which extends in an east-west direction, does not date to earlier than the 5th century and all units of the basilica are covered with stacks caused by collapse during the earthquake of AD 740 (Şahin et al., 2014a, 2014b). There is also a totally-submerged arc-shaped wall remnant extending from the north to the west of the basilica. It has not yet been determined whether the preserved wall structure, a few meters away from this basilica, was built to protect the city or basilica from the lake waters. Another question is whether this basilica was built on the ruins of an earlier church (Şahin and Fairchild, 2018) or the missing Temple of Apollo (Şahin, 2018a, 2018b). Fig. 6 is an aerial photograph showing the submerged basilica (Şahin et al., 2014b).

The aforementioned underwater archeology data state that no solid evidence has yet been reached on two issues; the structure upon which the underwater basilica was built, and the function of the arc-shaped "protection" wall. To try and answer these questions, geomorphological observations were made on the public beach outside the legal protection area of the basilica. Beachrock layers dipping toward the lake (westward) at an angle of around 5° provide an insight into the nature of the underlying unit of the basilica, when ledges perceived as being part of the plaster remains are considered (Şahin, 2018a, 2018b). Based on the fact that the subsurface nature of the beachrock layers may divulge information about the submerged parts, ERT measurements were made on the public beach about a meter away from the basilica foundations. The ERT profile, taken parallel to the shoreline along the beach and underwater, has also enabled us to provide insights into the collapse (?) of the 1600-year-old Byzantine Basilica of St. Neophytos.

Unlike the ERT profile shown in Fig. 4a, the ERT image taken on the public beach 5 m from the basilica area depicts low-angle beds dipping lakeward (westward) at an angle of 5° (Fig. 4b) Çınar et al., 2019. Resistivity values vary between 0 and 160 Ω.m and the maximum thickness of the buried beds is 1.5 m. Based on these results, no deformation structure was observed in the beachrock layers on the beach behind the basilica area. The buried beachrock identified in the ERT profile crops out along the shoreline as large blocks and extends to a depth of 2 m under the lake's surface. This implies that the base structure beneath the basilica is probably the most lakeward extension of this buried beachrock, rather than the remains of an earlier archaeological structure.

We suggest that the basilica must have been built on the layers of beachrock, comprising a hard platform on the shore when the lake level was about 2 m lower than at present due to drought. The multi-beam bathymetry of the lake (Gastineau et al., 2020), especially along the northern shores, indicates shorelines belonging to lowstands of the lake level driven by climate-related processes. This is confirmed by multi-proxy climatic data suggesting that consecutive arid stages occurred at 1.35 ka and 1.1 ka BP (Ülgen et al., 2012), which is compatible with evidence of consecutive cement fabrics typical of repeated drought stages in the Lake Iznik beachrocks (Öztürk et al., 2016). Since the basilica is located on the upthrown block of the offshore fault scarp (Gastineau et al., 2020), we propose that submergence of the 1.5 m-thick beachrock and remains of the basilica structure should be related to a rise in the lake's water level during the last 1500 years instead of earthquake-related subsidence in AD 740 or on another date.

6. Conclusions

Our structural analysis together with ERT data reveal that the original beachrock layers were displaced by a normal fault dipping north along a 100 m surface rupture. The absence of strike-slip deformation along the rupture indicates that this deformation occurred on a secondary structure away from the main fault. Most probably the main surface rupture was under the lake water. OSL ages of the deformed and undeformed layers constrain the timing of the earthquake to 1.3 ± 0.3 ka BP (8th century). There are two major earthquakes that temporally fit this date; those of AD 715 and AD 740. Historical records document severe damage to the city of Iznik during both of the earthquakes but the occurrence of a tsunami in the Marmara Sea during the AD 740 earthquake implies that it was an offshore earthquake, most probably along the offshore parts of the northern strand rather than the middle strand. Therefore, we suggest that the co-seismic deformation we found is geological evidence of the AD 715 earthquake and that this earthquake occurred along the middle strand.

Credit author statement

AEE detected the surface fracture, collected samples, interpreted the dating results, and wrote the article. RCE, OE and EU performed geophysical measurements and interpreted the results. CY, HHS and MK analyzed historical earthquake data and interpreted cosismic deformation. NGK performed optically stimulated luminescence dating methodology.

Declaration of Competing Interest

The authors declare that they have no known competing financial interests or personal relationships that could have appeared to influence the work reported in this paper.

Acknowledgements

This research was supported by TUBITAK (project no: 109Y143) and the Scientific Research Projects Unit of Çanakkale Onsekiz Mart University (project no: SBA-2018-2772). AEE wishes to thank the Turkish Academy of Sciences (TUBA) for their support in the framework of the GEBİP program. Nurettin Yakupoğlu is thanked for his help in calculating the radiocarbon reservoir ages of beachrock samples. This paper is dedicated in fond memory of Professor Cengiz Akbulak, who completed his doctoral studies in the Lake Iznik basin and sadly passed away on Sunday July 21, 2019.

References

Adatepe, F., Erel, L., 2006. İznik Tarihsel Dönem Deprem Verilerinin İrdelenmesi. İstanbul Üniv. Müh. Fak. Yerbilimleri Dergisi 19, 131–150.
Akbulak, C., 2006. İznik Depresyonu'nun Beşeri ve İktisadi Coğrafya Açısından İncelenmesi, (Doktora Tezi). İstanbul Üniversitesi, Sosyal Bilimler Enstitüsü, Coğrafya Anabilim Dalı, İstanbul.
Ambraseys, N.N., 2002. Seismic sea-waves in the Marmara Sea region during the last 20 centuries. J. Seismol. 6, 571–578.
Ambraseys, N.N., Finkel, C.F., 1991. Long-term seismicity of Istanbul and of the Marmara Sea region. Terra Nova 3, 527–539.
Ambraseys, N.N., Jackson, J.A., 1998. Faulting associated with historical and recent earthquakes in the Eastern Mediterranean region. Geophys. J. Int. 133, 390–406.
Antonopoulos, J., 1980. Data from investigation on seismic sea-waves events in the Eastern Mediterranean from 500 to 1000 A.D. Ann. Geofis. 33, 163–178.
Banerjee, D., Bøtter-Jensen, L., Murray, A.S., 1999. Retrospective Dosimetry: preliminary use of the single aliquot regeneration (SAR) protocol for the measurement of quartz dose in young house bricks. Radiat. Prot. Dosim. 84, 421–426.
Barka, A., 1993. Kuzey Anadolu Fayı'nın Sapanca-İzmit ve Geyve-İznik Kolları üzerinde Paleosismik Araştırmalar, Proje No:YBAG-4/7551. TÜBİTAK, İstanbul.
Bezerra, F.H.R., Lima-Filho, F.P., Amaral, R.F., Caldas, L.H.O., Costa-Neto, L.X., 1998. Holocene coastal tectonics. In: Stewart, I.S., Vitafinzi, C. (Eds.), Coastal Tectonics. The Geological Society, London, pp. 279–293.
Bøtter-Jensen, L., 1997. Luminescence techniques: instrumentation and methods. Radiat. Meas. 17, 749–768.
Çınar, H.E., Yılmaz, Turgal A., Erginal, A.E., Erenoğlu, O., Ulugergerli, E.U., Erenoğlu, R. C., 2019. Is submergence of the saint neophytos basilica (Lake İznik, NW Turkey) caused by AD 740 earthquake or climate change? Discussion of geoelectrical data. In: International Conferences on Science and Technology ICONST 2019, Prizren, Kosova, 26–30 August 2019, vol.1, no.1, pp. 513–521.

Doğan, B., Tüysüz, O., Şanlı, F.B., 2015. Tectonostratigraphic evolution of the basins on the southern branch of the North Anatolian Fault System in the SE Marmara Region, Turkey. International Journal of Earth Sciences 104(2), 389–418.

Emre, Ö., Duman, T.Y., Özalp, S., Elmacı, H., Olgun, Ş., Şaroğlu, F., (2013). Açıklamalı Türkiye Diri Fay Haritası, Ölçek 1:1.250.000, Maden Tetkik ve Arama Genel Müdürlüğü, Özel Yayın Serisi: 30, 89 s., Ankara.

Ergin, K., Güçlü, U., Uz, Z., 1967. Türkiye ve Civarının Deprem Kataloğu (Milattan Önce 11 yılından 1964 sonuna kadar). İ.T.Ü. Maden Fakültesi, Arz Fizigi Enstitüsü Yayınları, İstanbul.

Erginal, A.E., 2017. Iznik Gölü'nün Fosil Plajları (Yalıtaşları) / Fossil Beaches of Lake İznik (Beachrocks). Çantay Yayınevi, İstanbul.

Erginal, A.E., Kiyak, N.G., Ozturk, M.Z., Yigitbas, E., Bozcu, M., Avcioglu, M., 2012a. First note on marine-like cementation of late Holocene beachrock, Iznik Lake (Turkey). Geochronometria 39, 76–83.

Erginal, A.E., Kiyak, N.G., Ozturk, M.Z., Avcioglu, M., Bozcu, M., Yigitbas, E., 2012b. Cementation characteristics and age of beachrocks in a fresh-water environment, Lake Iznik, NW Turkey. Sediment. Geol. 243-244, 148–154.

Fraser, J., Vanneste, K., Hubert-Ferrari, A., 2010. Recent behavior of the North Anatolian Fault: insights from an integrated paleoseismological data set. J. Geophys. Res. B09316 https://doi.org/10.1029/2009JB006982.

Gastineau, R., Sigoyer, J.De., Sebatier, P., Fabbri, S.C., Anselmetti, F.S., Develle, A.L., Şahin, M., Gündüz, S., Niessen, F., Gebhardt, A.C., 2020. Active subaquatic fault segments in Lake Iznik along the middle strand of the North Anatolian Fault, NW Turkey. In: Earth and Space Science Open Archive (ESSOAr). https://doi.org/10.1002/essoar.10504104.1.

Guidoboni, E., Comastri, A., Traina, G., 1994. Catalogue of Ancient Earthquakes in the Mediterranean Area up to the 10th Century, vol. 1. ING-SGA, Bologna.

https://www.oca.org/saints/lives/2016/10/26/103060-commemoration-of-the-great-earthquake-at-constantinople. Last access: 24.10.2020.

Ikeda, Y., Suzuki, Y., Herece, E., Şaroğlu, F., Işıkara, A.M., Honkura, Y., 1991. Geological evidence for the last two faulting events on the North Anatolian Fault Zone in the Mudurnu Valley, Western Turkey. Tectonophysics 193, 335–345.

Kayan, İ., 1996. İznik Gölü batısındaki Ilıpınar Höyüğü çevresinde jeomorfolojik ve jeo-arkeolojik araştırmalar. Ege Coğrafya Dergisi 9, 43–70.

Kelletat, D., 2006. Beachrock as a sea-level indicator? Remarks from a geomorphological point of view. J. Coast. Res. 22, 1555–1564.

Kozacı, Ö., Dolan, J.F., Yönlü, Ö., Hartleb, R.D., 2011. Paleoseismologic evidence for the relatively regular recurrence of infrequent, large-magnitude earthquakes on the eastern North Anatolian fault at Yaylabeli Turkey. Lithosphere 3, 37–54.

Loke, M.H., 2004. Tutorial: 2-D and 3-D Electrical Imaging Surveys. http://personales.upv.es/jpadin/coursenotes.pdf.

Loke, M.H., 2013. Tutorial: 2D and 3D Electrical Imaging Surveys. http://www.geotomosoft.com/coursenotes.zip (accessed 05 April 2013).

Murray, A.S., Wintle, A.G., 2000. Luminescence dating of quartz using an improved single-aliquot regenerative-dose protocol. Radiat. Meas. 32, 57–73.

Neyamadpour, A., Wan Abdullah, V.A.T., Samsudin, T., Neyamadpour, B., 2010. Comparison of Wenner and dipole–dipole arrays in the study of an underground three-dimensional cavity. J. Geophys. Eng. 7 (1), 30–40.

Olley, J.M., Murray, A.S., Robert, R.G., 1996. The effects of disequilibria in the uranium and thorium decay chain on burial dose rates in fluvial sediments. Quat. Sci. Rev. 15, 751–760.

Özalp, S., Emre, Ö., Doğan, A., 2013. Kuzey Anadolu Fayı Güney Kolu'nun segment yapısı ve Gemlik Fayı'nın Paleosismik Davranışı, KB Anadolu. MTA Dergisi 147, 1–17.

Öztürk, K., Yaltırak, C., Alpar, B., 2009. The relationship between the tectonic setting of the Lake Iznik basin and the middle strand of the North Anatolian Fault. Turk. J. Earth Sci. 18, 209–224.

Öztürk, M.Z., Erginal, A.E., Kiyak, N.G., Öztürk, T., Demirci, A., Ekinci, Y.L., Cürebal, İ., Avcıoğlu, M., Öztürk, T., 2016. Records of repeated drought stages during the Holocene, Lake Iznik (Turkey) with reference to beachrock. Quat. Int. 408, 16–24.

Pınar Erdem, N., Lahn, E., 2001. Türkiye Depremleri İzahlı Kataloğu, 2. Basım, Yıldız Teknik Üniversitesi Vakfı Yayınları, İstanbul.

Prescott, J.R., Hutton, J.T., 1988. Cosmic ray and gamma ray dosimetry for TL and ESR. Nucl. Tracks Radiat. Measur. 14, 223–227.

Prescott, J.R., Hutton, J.T., 1994. Cosmic ray contribution to dose rates for luminescence and ESR dating: large depths and long-term time variations. Radiat. Meas. 23, 497–500.

Reilinger, R., McClusky, S., Vernant, P., Lawrence, S., Ergintav, S., Cakmak, R., Ozener, H., Kadirov, F., Guliev, I., Stepanyan, R., Nadariya, M., Hahubia, G., Mahmoud, S., Sakr, K., ArRajehi, A., Paradissis, D., Al-Aydrus, A., Prilepin, M., Guseva, T., Evren, E., Dmitrotsa, A., Filikov, S.V., Gomez, F., Al-Ghazzi, R., Karam, G., 2006. GPS constraints on continental deformation in the Africa–Arabia–Eurasia continental collision zone and implications for the dynamics of plate interactions. J. Geophys. Res. 111, B05411. https://doi.org/10.1029/2005JB004051.

Roeser, P., 2014. Paleolimnology of Lake Iznik (NW Turkey) during the past ~ 31 ka cal BP, PhD thesis. Rheinische Friedrich-WilhelmsUniversität Bonn, Bonn, 202 pp.

Şahin, M., 2018a. Hava fotoğrafları ve arkeoloji biliminde yeni bir keşif İznik Gölü Bazilikası. Yükseköğretim Dergisi 9, 78–81.

Şahin, M., 2018b. İznik Gölü bazilika kazıları 2017-2018. TINA Denizcilik Arkeolojisi Dergisi 10, 116–126.

Şahin, M., Fairchild, M.R., 2018. Nicea's underwater basilica. Biblic. Archaeol. Rev. 44, 30–38.

Şahin, M., Tok, E., Kılıç, Ş., 2014a. Deprem kurbanı Aziz Neophytos: İznik Gölü'ndeki batık kilise. Deniz Mag. 39, 42–45.

Şahin, M., Tok, E., Kılıç, Ş., 2014b. İznik, Göldeki Bazilika. https://www.atlasdergisi.com/kesfet/arkeoloji/iznik-goldekibazilika.html (accessed 29 November 2019).

Şengör, A.M.C., Tüysüz, O., İmren, C., Sakınç, M., Eyidoğan, H., Görür, N., Le Pichon, X., Rangin, C., 2005. The North Anatolian Fault: A new look. Annu. Rev. Earth Planet. Sci. 33, 37–112.

Soysal, H., Sipahioglu, S., Kolçak, D., Altınok, Y., 1981. Türkiye ve Çevresinin Tarihsel Deprem Kataloğu, (M.O. 2100- M.S. 1900). TÜBİTAK, İstanbul.

Ülgen, U.B., Franz, S.O., Biltekin, D., Çagatay, M.N., Roeser, P.A., Doner, L., Thein, J., 2012. Climatic and environmental evolution of Lake Iznik (NW Turkey) over the last ~4700 years. Quat. Int. 274, 88–101.

Vousdoukas, M.I., Velegrakis, A.F., Plomaritis, T.A., 2007. Beachrock occurrence, characteristics, formation mechanism and impacts. Earth Sci. Rev. 85, 23–46.